Inorg. Chem. **2002**, *41*, 5721–5732

Redox and Spectroscopic Orbitals in Ru(II) and Os(II) Phenolate Complexes

Tia E. Keyes,*,† Deirdre Leane,† Robert J. Forster,‡ Colin G. Coates,§ John J. McGarvey,§ Mark N. Nieuwenhuyzen,§ Egbert Figgemeier,|| and Johannes G. Vos*,‡

School of Chemistry, Dublin Institute of Technology, Dublin 8, Ireland, School of Chemical Sciences, Dublin City University, Glasnevin, Dublin 9, Ireland, School of Chemistry, The Queens University of Belfast, Belfast, Northern Ireland, and Department of Physical Chemistry, Uppsala University, P.O. Box 532, S-751 21 Uppsala, Sweden

Received April 2, 2002

A detailed spectroscopic and electrochemical study of a series of novel phenolate bound complexes, of general formulas $[M(L\text{-}L)_2(box)](PF_6)$, where M is Os and Ru, L-L is 2,2-bipyridine or 2,2-biquinoline, and box is 2-(2-hydroxyphenyl)benzoxazole, is presented. The objectives of this study were to probe the origin of the LUMOs and HOMOs in these complexes, to elucidate the impact of metal and counter ligand on the electronic properties of the complex, and to identify the extent of orbital mixing in comparison with considerably more frequently studied quinoid complexes. $[M(L\text{-}L)_2(box)](PF_6)$ complexes exhibit a rich electronic spectroscopy extending into the near infrared region and good photostability, making them potentially useful as solar sensitizers. Electrochemistry and spectroscopy indicate that the first oxidation is metal based and is associated with the M(II)/(III) redox states. A second oxidative wave, which is irreversible at slow scan rates, is associated with the phenolate ligand. The stabilities of the oxidized complexes are assessed using dynamic electrochemistry and discussed from the perspective of metal and counter ligand (LL) identity and follow the order of increasing stability $[Ru(biq)_2(box)]^+ < [Ru(bpy)_2(box)]^+ < [Os(bpy)_2(box)]^+$. Electronic and resonance Raman spectroscopy indicate that the lowest energy optical transition for the ruthenium complexes is a phenolate (π) to L-L (π^*) interligand charge-transfer transition (ILCT) suggesting the HOMO is phenolate based whereas electrochemical data suggest that the HOMO is metal based. This unusual lack of correlation between redox and spectroscopically assigned orbitals is discussed in terms of metal–ligand orbital mixing which appears to be most significant in the biquinoline based complex.

Introduction

The application of metal complexes as photo- and electrochromic materials requires that electronic spectral features lie within useful, often visible ranges. The same requirement is made for application of such species in solar energy devices where the objective is optimal superimposition of the electronic spectra with the solar energy flux.

There has been significant interest in Ru/Os−O^- coordinated quinoid ligands as a consequence of their noninnocent redox behavior and rich visible−NIR spectroscopy. $Ru(bpy)_2$ based complexes bound to O^- bearing ligands, such as catechols or hydroquinones, have been shown to possess strong charge-transfer transitions in the visible and NIR spectral regions. Typically, in such complexes, the higher energy visible region, 400−500 nm, is dominated by bands associated with MLCT Ru(II)−bpy(π^*) transitions, whereas at lower energy, i.e., >500 nm, transitions are ascribed to considerably less common interligand charge-transfer, ILCT.[1] There have, however, been comparably few reports of such complexes in which the coordinated O is donated from a phenolate.[2,3] Like the quinoids, these are anticipated to be noninnocent ligands capable of coordinating via an anionic oxygen donor in their reduced state. In general, the oxidation

* To whom correspondence should be addressed. E-mail: Tia.Keyes@dcu.ie (T.E.K.).
† Dublin Institute of Technology.
‡ Dublin City University.
§ The Queens University of Belfast.
|| Uppsala University.

(1) Keyes, T. E.; Jayaweera, P. M.; McGarvey, J. J.; Vos, J. G. *J. Chem. Soc., Dalton Trans.* **1997**, 1627.
(2) Basuli, F.; Peng, S. M.; Bhattacharya, S. *Polyhedron* **1998** *18*, 391.
(3) Dutta, S.; Peng, S. M.; Bhattacharya, S. *J. Chem. Soc., Dalton Trans.* **2000**, 4623.

10.1021/ic0202561 CCC: $22.00
Published on Web 10/05/2002

Scheme 1. Structure of box Ligand Illustrating Numbering Scheme for ^{1}H NMR Data

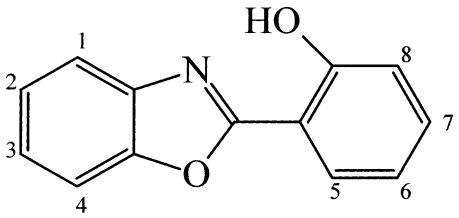

potentials of phenols are anticipated to be higher than those of their quinoid counterparts.

We are interested in phenolate donors for three reasons: First, as strong σ-donors, they are capable of increasing the photochemical stability of Ru(II) complexes while simultaneously extending the visible absorbance range of the complex through ILCT transitions. Second, significant research has been dedicated to catecholate and quinone based Ru and Os O−O and O−N bound complexes. However, the influence of the reduced ligand on the metal redox levels is not apparent in these systems because the ligand oxidation is more facile than the metal. The higher oxidation potentials of the phenolate described here allows us to directly study the M−O$^-$ behavior from the perspective of the metal. Such studies provide us with the opportunity of investigating directly the redox behavior of the metal when bound to anionic oxygen. Finally, a feature of O bound catecholate and quinoid ligands seems to be significant metal−ligand orbital mixing. We were interested in investigating if this behavior is limited to quinoid ligands or typical of aryl O$^-$ donor ligands in general.

In this paper, we report on three complexes, $[Ru(bpy)_2(box)]^+$, $[Os(bpy)_2(box)]^+$, and $[Ru(biq)_2(box)]^+$, where bpy is 2,2-bipyridine, biq is 2,2-biquinoline, and box is 2-(2-hydroxyphenyl)benzoxazole (Scheme 1). The use of bipyridyl and biquinoline derivatives allows the influence of the identity of both the metal and counter ligand on optical transitions and electrochemistry of these phenolate based complexes to be addressed. We provide a detailed assignment of the electrochemistry and optical spectroscopic properties of these complexes on the basis of potential controlled electronic and resonance Raman spectroscopy. We discuss the influence of acceptor ligands and metal on optical transitions and illustrate how, by judicious choice of ligand, we can manipulate the spectral region over which the transition will occur. We illustrate and discuss an interesting lack of agreement between redox assigned and spectroscopically assigned location of the HOMO on the bipyridyl based complex and ascribe this behavior to strong ligand−metal orbital mixing.

Experimental Section

Materials. d_8-bpy was synthesized according to published methods.[4] Dichloride complexes, *cis*-$Ru(bpy)_2Cl_2$, $Ru(d_8\text{-bpy})_2Cl_2$, $Os(bpy)_2Cl_2$, $Ru(d_8\text{-bpy})_2Cl_2$, $Ru(biq)_2Cl_2$, were synthesized by standard methods.[5−7] All other reagents, purchased from Sigma-Aldrich, were used as received.

Absorption spectra were measured using a Shimadzu 3500 UV−vis−NIR spectrophotometer. Spectra were fitted to Gaussian curves using standard iterative algorithms.[8]

Electrochemical studies were conducted in HPLC grade solvents, dried over molecular sieves, 3 Å; 0.1 M tetraethylammonium tetrafluoroborate ($TeaBF_4$) was used as the supporting electrolyte.

Cyclic voltammetry was carried out using a CH instruments model 660 electrochemical workstation. Cells were of conventional design and were thermostated to within ±0.2 °C using a Julabo F10-HC refrigerated circulating bath. All potentials are quoted with respect to a BAS Ag/AgCl organic reference electrode. Under the conditions employed, the oxidation potential of ferrocene was +0.312 V versus Ag/AgCl. All solutions were degassed using nitrogen, and a blanket of nitrogen was maintained over the solution during all experiments. Platinum microwires (Goodfellow Metals Ltd.) of radii between 5 and 25 μm were sealed in soft glass as described previously.[9] Microdisk electrodes were exposed by removing excess glass using 600 grit emery paper followed by successive polishing with 12.5, 5, 1, 0.3, and 0.05 μm alumina. The polishing material was removed between changes of particle size by sonicating the electrodes in deionized water for at least 5 min. The polished electrodes were electrochemically cleaned by cycling in 0.1 M $HClO_4$ between potential limits chosen first to oxidize and then to reduce the surface of the platinum electrode. Finally, the electrode was cycled between −0.300 and 0.700 V in 0.1 M $NaClO_4$ until hydrogen desorption was complete.

Spectroelectrochemistry was carried out using a homemade Pyrex glass, thin layer cell (1 mm). The optically transparent working electrode was a platinum gauze, which was inserted fully into the cell; the auxiliary electrode was a platinum wire, and the reference was Ag/AgCl. Solvent and electrolyte were as described previously. The working electrode was held at the required potential throughout the measurement using an EG&G PAR model 362 scanning potentiostat. Absorption spectra were obtained on a Shimadzu 3500 UV−vis−NIR spectrophotometer.

Resonance Raman experiments were recorded using an Ar^+ laser as the excitation source in the region 355 to 528 nm and a Ti-sapphire laser pumped by an Ar^+ laser for experiments carried out at wavelengths beyond 700 nm. A backscattering geometry was employed for the spectral accumulations using a liquid nitrogen cooled CCD multichannel detector coupled to a single stage monochromator (JY640HD). A holographic notch filter was used at the entrance slit to minimize Rayleigh scattering. Alternatively, Raman spectroscopy was conducted on a Dilor.Jobinyvon.Spex Labram. The exciting 20 mW helium−neon laser (632.8 nm) or Ar ion laser (514 nm) was focused through the thin layer electrochemical cell onto the surface of the optically transparent platinum/rhodium gauze surface using a 10× objective lens. Focusing was confirmed by using an imaging video camera. A spectral resolution of 1.5 cm^{-1} per pixel was achieved using a grating of 1800 lines/mm. The applied potential was controlled with respect to an SCE reference electrode using a CH instruments model

(4) Keyes, T. E.; Weldon, F.; Muller; Pechy, E. P.; Gratzel, M.; Vos, J. G. *J. Chem. Soc., Dalton Trans.* **1995**, 2705.

(5) Sullivan, B. P.; Salmon, D. J.; Meyer, T. J. *Inorg. Chem.* **1978**, *17*, 3334.

(6) Lay, P. A.; Sargeson, A. M.; Taube, H.; Chou, M. H.; Creutz, C. *Inorg. Synth.* **1986**, *24*.

(7) Keyes, T. E.; Vos, J. G.; Kolnaar, J. A.; Haasnoot, J.; Reedijk, J.; Hage, R. *Inorg. Chim. Acta* **1996**, *237*, 245.

(8) Diamond, D.; Hanratty, V. *Excel for Chemists*; John Wiley & Sons: VCH, 1997.

(9) (a) Faulkner, L. R.; Walsh, M. R.; Xu, C. *Contemporary Electroanalytical Chemistry*; Plenum Press: New York, 1990. (b) Xu, C. Ph.D. Thesis, University of Illinois at Urbana-Champaign, 1992. (c) Forster, R. J.; Faulkner, L. R. *J. Am. Chem. Soc.* **1994**, *116*, 5444.

600A potentiostat or oxidation was achieved chemically using cerium sulfate.

Complex Synthesis. [Ru(bpy)$_2$(box)](PF$_6$)·(CH$_3$CN). [Ru(bpy)$_2$Cl$_2$]·2H$_2$O (0.676 g, 1.3 mmol) was dissolved in ethanol/water (1:1 v/v, 40 cm^3) containing diethylamine (2%, v/v). This solution was deoxygenated with argon and heated, and box dissolved (0.12 g, 0.6 mmol) in ethanol/water (1:1 v/v, 40 cm^3) (2% DEA) was added slowly over 20 min. The mixture was heated under reflux in an argon atmosphere for 4 h after which time the burgundy solution was reduced in volume to approximately 10 cm^3 and neutralized with sulfuric acid. After neutralization, the solution was allowed to stand for several hours and then filtered to remove any salt formed. Several drops of saturated aqueous NH_4PF_6 were subsequently added to the solution, and the resulting burgundy crystals were collected by filtration. The product was recrystallized twice from acetonitrile/water 3:2 v/v. Yield 65%. Anal. Calcd for [Ru(bpy)$_2$(box)](PF$_6$)·CH$_3$CN, $RuC_{35}H_{28}N_6O_2PF_6$: C, 51.66; H, 3.44; N, 10.32. Found: C, 51.58; H, 3.47; N, 10.02. ^{1}H NMR of box related resonances (400 MHz, CD_3CN): H^3, H^4, 7.13 (m 2H); H^5, H^6, H^7, 7.39 (m, 3 H); H^1, H^2, 7.75 (m, 2H); H^8, 7.93 (d, 1H).

[Ru(d_8-bpy)$_2$(box)](PF$_6$). [Ru(bpy)$_2$(box)](PF$_6$) was synthesized and purified as described for [Ru(bpy)$_2$(box)](PF$_6$) starting with Ru(d_8-bpy)$_2$Cl$_2$; the complex was obtained as a dark burgundy powder. Yield 68%. ^{1}H NMR box related resonances (400 MHz, CD_3CN): H^3, H^4, 7.10 (m 2H); H^5, H^6, H^7, 7.39 (m, 3 H); H^1, H^2, 7.73 (m, 2H); H^8, 7.93, (d, 1H).

[Os(bpy)$_2$(box)](PF$_6$). [Os(bpy)$_2$(box)](PF$_6$) was synthesized and purified as described for [Ru(bpy)$_2$(box)](PF$_6$) starting with Os(bpy)$_2$Cl$_2$, except the reflux was conducted over 8 h; the complex was obtained as a dark purple-brown powder. Yield 60%. Anal. Calcd for $OsC_{33}H_{25}N_5O_2PF_6$: C, 46.04; H, 2.91; N, 8.13. Found: C, 45.38; H, 3.11; N, 8.21.

^{1}H NMR box related resonances (400 MHz, CD_3CN): H^3, H^4, 7.03 (m 2H); H^5, H^6, H^7, 7.39 (m, 3 H); H^1, H^2, 7.71 (m, 2H); H^8, 7.93 (d, 1H).

[Os(d_8-bpy)$_2$(box)](PF$_6$). [Os(bpy)$_2$(box)](PF$_6$) was synthesized and purified as described for [Os(bpy)$_2$(box)](PF$_6$) starting with Os(d_8-bpy)$_2$Cl$_2$; the complex was obtained as a dark purple-brown powder, yield, 58%. ^{1}H NMR box related resonances (400 MHz, CD_3CN): H^3, H^4, 7.06 (m 2H); H^5, H^6, H^7, 7.40 (m, 3 H); H^1, H^2, 7.71 (m, 2H); H^8, 7.92 (d, 1H).

[Ru(biq)$_2$(box)](PF$_6$). [Ru(biq)$_2$(box)](PF$_6$) was synthesized as described for [Ru(bpy)$_2$(box)](PF$_6$) starting with Ru(biq)$_2$Cl$_2$. The complex was obtained as a purple powder. Yield 60%. Calcd for $RuC_{49}H_{33}N_5O_2PF_6$: C, 61.5; H, 3.51; N, 7.22. Found: C, 60.8; H, 3.47; N, 7.96. ^{1}H NMR (400 MHz) box related resonances (400 MHz, CD_3CN): H^3, 6.58 (d 1H); H^5, H^6, H^7, 7.28 (m, 3 H); H^1, H^2, H^4, 7.58 (m, 2H); H^8, 8.14, (d, 1H).

Crystal Structure Determination. Crystals of [Ru(bpy)$_2$(box)](PF$_6$) were grown by slow evaporation of an acetonitrile/water solution, 2:1 v/v. Data were collected on a (0.54 × 0.21 × 0.18 mm^3) crystal.

Crystallographic data were collected on a Siemens P4 diffractometer using the XSCANS[10] software with graphite monochromated Mo Kα radiation using ω scans. A crystal was mounted onto the diffractometer at low temperature under dinitrogen at ca. 120 K. Crystal stability was monitored by measuring standard reflections every 100 reflections, and there were no significant variations (<±1%). Cell parameters were obtained from 35 accurately centered reflections in the 2θ range 10−25°. ω scans were employed for data collection, and Lorentz and polarization corrections were applied. An empirical absorption correction using ψ scans was applied to [Ru(bpy)$_2$(box)](PF$_6$).

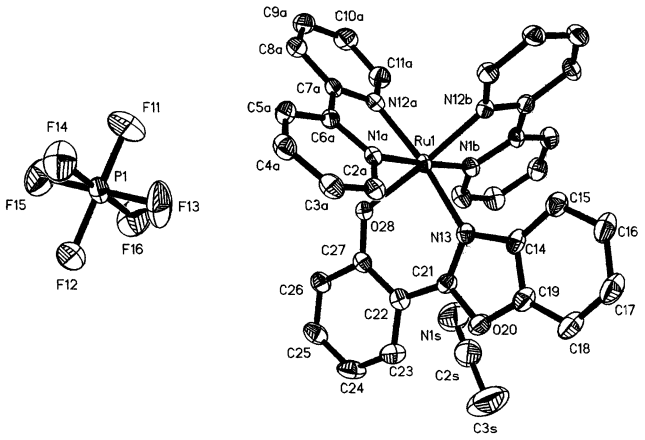

Figure 1. Crystal Structure of [Ru(bpy)$_2$(box)](PF$_6$) showing numbering scheme and counterion.

The structure was solved using direct methods with the SHELXTLPC and SHELXL-93 program packages,[11] and the non-hydrogen atoms were refined with anisotropic thermal parameters. Hydrogen atom positions were located from difference Fourier maps, and a riding model with fixed thermal parameters ($U_{ij} = 1.2U_{eq}$ for the atom to which they are bonded) was used for subsequent refinements. The function minimized was $\sum[w(|F_o|^2 - |F_c|^2)]$ with reflection weights $w^{-1} = [\sigma^2 |F_o|^2 + (g_1P)^2 + (g_2P)]$ where $P = [\max|F_o|^2 + 2|F_c|^2]/3$.

Crystal data for [Ru(bpy)$_2$(box)](PF$_6$)·(CH$_3$CN): MW = 809.67, monoclinic, space group $P2_1/c$, a = 8.959(2) Å, b = 13.930(2) Å, c = 26.737(5) Å, β = 92.07(2)°, U = 3334.6 (11) Å^{-3}, Z = 4, μ = 0.595 mm^{-1}, R_{int} = 0.0155 A total of 6261 reflections were measured for the angle range $4 < 2\theta < 50$, and 5860 independent reflections were used in the refinement, transmission range (max, min) = 0.9712, 0.8935. The final parameters were wR2 = 0.0724 and R1 = 0.0291 [$I > 2\sigma I$].

Semiempirical calculations were performed using the program package ZINDO within the INDO/S-CI framework, which had been parametrized to reproduce spectroscopic properties of ruthenium complexes.[12] The geometries for [Ru(bpy)$_2$(box)]$^+$ were taken from the crystal coordinates, and only single point calculations were carried out, whereas for [Ru(biq)$_2$(box)]$^+$ molecular mechanics geometry optimizations were conducted prior to calculation.

Results and Discussion

Structural Characterization. The complexes were synthesized according to standard techniques; addition of base was necessary to deprotonate the hydroxyl group and render it a better coordination site. Complexes were obtained in high yield and were found to be greater than 98% pure on HPLC after two recrystallizations. The structure of the [Ru(bpy)$_2$(box)]PF$_6$ complex was determined by X-ray crystallography and is shown in Figure 1. The asymmetric unit contains one [Ru(bpy)$_2$(box)](PF$_6$) ion pair and a molecule of acetonitrile. The box anion is coordinated to ruthenium as a bidentate N,O-donor forming a five-membered chelate ring, and the

(10) Fait, J. *XSCANS, System for Data Collection*; Bruker-AXS: Madison, WI, 1993.

(11) Sheldrick, G. M. *SHELXLPC, A System for Structure Solution and Refinement*; Bruker-AXS: Madison, WI, 1998.

(12) Rensmo, H.; Lunell, S.; Siegbahn, H. *J. Photochem. Photobiol., A* **1998**, *114*, 117.

Table 1. Selected Bond Distances (Å) and Angles (deg) for $[Ru(bpy)_2(box)](PF_6)\cdot CH_3CN$

Ru(1)-N(12B)	2.031(2)	Ru(1)−N(1A)	2.048(2)
Ru(1)−N(12A)	2.041(2)	Ru(1)−O(28)	2.0569(18)
Ru(1)−N(1B)	2.046(2)	Ru(1)−N(13)	2.093(2)
N(12A)−Ru(1)−N(13)	171.95(8)	O(28)−Ru(1)-N(13)	89.30(8)
N(1B)-Ru(1)−N(13)	87.21(8)	N(12B)−Ru(1)−N(12A)	88.65(8)
N(1A)−Ru(1)−N(13)	94.87(8)	N(12B)−Ru(1)−N(1B)	79.20(8)
N(12A)−Ru(1)−N(1B)	99.19(8)	N(12B)−Ru(1)−N(1A)	99.21(8)
N(12A)−Ru(1)−N(1A)	78.85(8)	N(1B)−Ru(1)−N(1A)	177.54(8)
N(12B)−Ru(1)−O(28)	170.48(8)	N(12A)−Ru(1)−O(28)	85.37(8)
N(1B)−Ru(1)−O(28)	94.43(8)	N(1A)−Ru(1)−O(28)	86.90(8)
N(12B)−Ru(1)−N(13)	97.39(8)		

RuN_5O coordination sphere is distorted octahedral, typical of these bidentate ligands, Table 1. The $[Ru(bpy)_2(box)]$ cations form an extended array via a combination of C−H···π and $\pi\cdots\pi$ interactions and C−H···O hydrogen bonds. This leads to the formation of channels along the *a* axis in which the anions and solvent molecules are located, Figure 2.

In $[Ru(bpy)_2(box)](PF_6)$, the PF_6 anions within the channels are involved in a significant number of short contacts (2.3−2.9 Å) with the C−H moieties of the $[Ru(bpy)_2(box)]$ cations and the methyl groups of the acetonitrile molecules. This is consistent with the formation of C−H···F hydrogen bonds between the cations and anions and in agreement with a database study on organometallic compounds containing fluorinated anions by Bragga et al.[13] showing that both BF_4^- and PF_6^- anions can act as conventional hydrogen bond acceptors. They concluded that C−H···F hydrogen bonds to BF_4^- and PF_6^- anions are significant for the formation of many crystalline materials.

This structural configuration, where anions exist within channels in the crystal, is particularly interesting from the perspective of the solid state behavior of similar materials. We recently reported on the solid state electrochemistry of O,N coordinated Ru and Os complexes bound to hydroquinone; the crystallography of these materials was not available, but it was speculated that such a porous structure might account for the excellent conductivity of these materials in their solid states.[14]

The complexes are diamagnetic, and accordingly, sharp, well defined ^{1}H NMR resonances were observed for all complexes, consistent with the presence of both M(II) and the phenolate as reduced species. A complete assignment of all box based resonances could be made by employing a combination of COSY ^{1}H NMR experiments and deuteriation of bipyridine;[4] these are presented in the synthetic section. Identification of individual biquinoline and bipyridine was not undertaken; however, integration of NMR spectra was correct for each complex.

Spectroscopy. Electronic Spectroscopy. All three complexes reveal strong CT transitions across the entire visible region, as shown in Figure 3. $[Ru(bpy)_2(box)]^+$ exhibits a strong absorbance with a λ_{max} of 488 nm (ϵ = 8695 M^{-1} cm^{-1}), and a weaker shoulder, which from Gaussian fitting,[8] appears to be centered at 550 nm (ϵ = 1150 M^{-1} cm^{-1}); this broader band extends to nearly 750 nm. The main absorbance feature for $[Os(bpy)_2(box)]^+$ is at 520 nm (ϵ = 9244 M^{-1} cm^{-1}); this band is also broadened and would appear to overlay the same broad feature observed in the analogous Ru complex. A broad, non-Gaussian absorbance with a λ_{max} of 720 nm (ϵ = 3031 M^{-1} cm^{-1}) is also observed and is most likely associated with the ^{3}MLCT (Os to bpy π^*) transition rendered allowed by spin−orbit coupling of the heavy Os atom.[15] $[Ru(biq)_2(box)]^+$ exhibits intense visible absorbances which extend beyond 800 nm. The main feature, with a λ_{max} of 600 nm (ϵ = 3031 M^{-1} cm^{-1}), is superimposed on a broad underlying shoulder identified from spectral fitting as centered at 670 nm (ϵ = 1583 M^{-1} cm^{-1}).

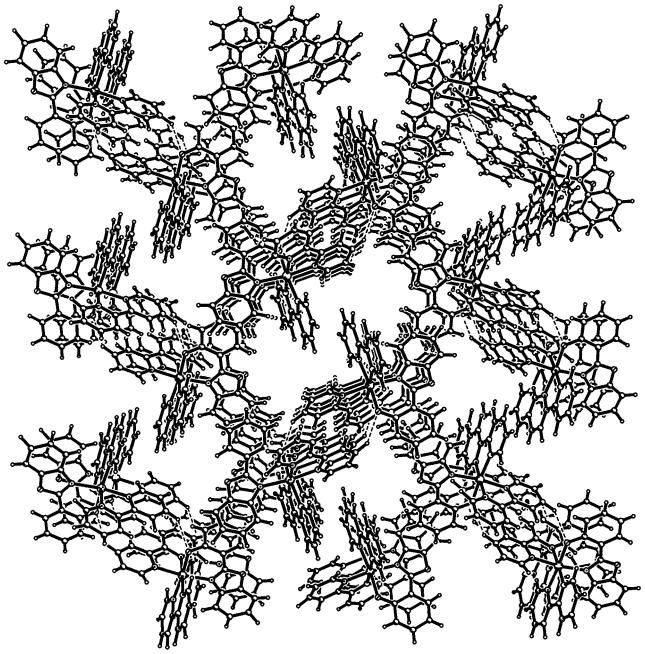

Figure 2. View down the *a* axis showing the channels formed by the cations in **1**. The anions and solvent molecules have been removed for clarity.

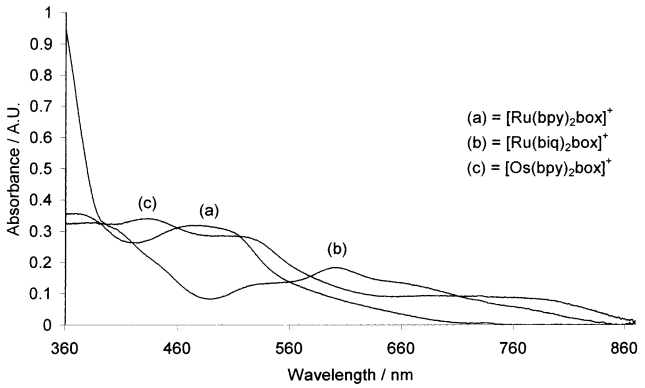

Figure 3. UV−vis absorption spectra of $[M(L\text{-}L)_2(box)]^+$ complexes in acetonitrile solution.

Raman Spectroscopy. Raman spectroscopy was carried out to elucidate the origin of the optical transitions, in each

(13) Grepioni, F.; Cojazzi, G.; Draper, S. M.; Scully, N.; Braga, D. *Organometallics* **1998**, *17*, 296.
(14) Bond, A. M.; Marken, F.; Williams, C. T.; Beattie, D. A.; Keyes, T. E.; Forster, R. J.; Vos, J. G. *J. Phys. Chem. B* **2000**, *104*, 1977.
(15) Hupp, J. T.; Neyhart, G. A.; Meyer, T. J. *J. Am. Chem. Soc.* **1986**, *108*, 5349.

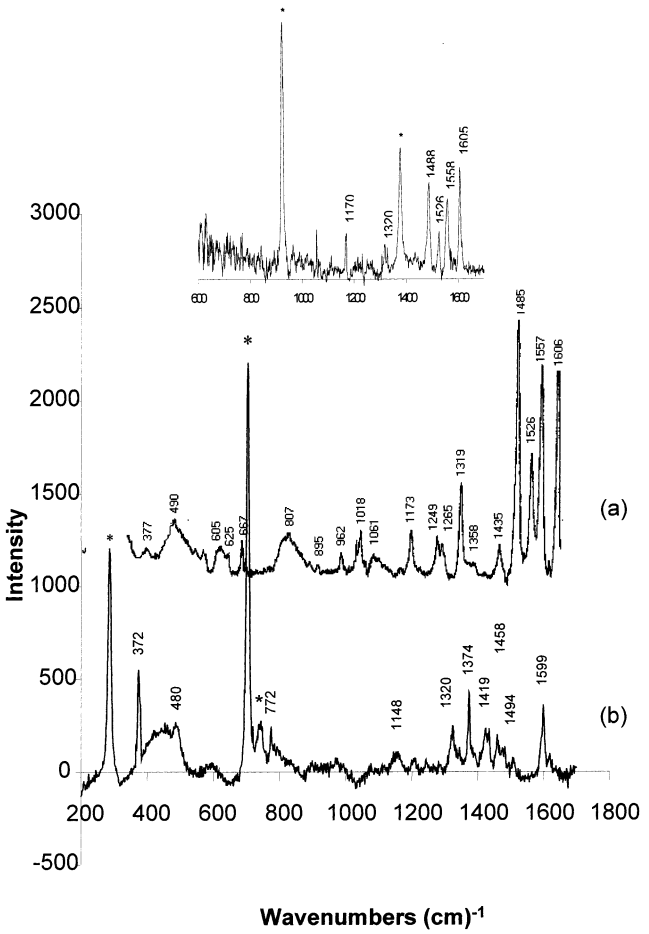

Figure 4. Resonance Raman of (a) $[Ru(bpy)_2(box)]^+$ excited at 632.8 nm in dichloromethane and (b) $[Ru(biq)_2(box)]^+$ excited at 514 nm in dichloromethane. Inset: $[Ru(bpy)_2(box)]^+$ excited at 457.9 nm in acetonitrile.

instance employing excitation wavelengths that were coincident with the absorbances under interrogation. Under such conditions, the Franck−Condon modes of the chromophore are resonantly enhanced by up to 7 orders of magnitude. This provides a valuable means of identifying the origin of optical transitions.

Figure 4 (inset) shows the Raman spectrum of $[Ru(bpy)_2(box)]^+$ using 457.9 nm excitation which is resonant with the 488 nm absorbance of this complex. The spectrum exhibits bands typically expected for resonance with a Ru (dπ)−bpy (π*) MLCT transition with enhancement of bipyridyl vibrations, at 1605, 1558, 1488, 1320, 1170, and 1023 cm^{-1}, and a Ru−N vibration is also observed at 377 cm^{-1}.[16] The relatively strong feature at 1526 cm^{-1} and features at approximately 1475 and 1600 cm^{-1}, obscured by the bpy features at 1605 and 1558 cm^{-1}, are attributed to the box ligand because they are insensitive to deuteriation of the bipyridyl moieties. Furthermore, these bands are not observed in the resonance Raman spectrum for typical MLCT transitions of $[Ru(bpy)_3]^{2+}$. The appearance of box vibrations is attributed to the fact that the 457.9 nm excitation falls within the tail of a box based intraligand $\pi-\pi$* transition. Such an effect has been reported previously for hydroquinone based complexes.[1]

The Raman spectrum of $[Ru(bpy)_2(box)]^+$ excited at 632.8 nm is shown in Figure 4a. The 632.8 nm excitation is resonant with the shoulder centered at 550 nm, but at this wavelength, any contribution from the MLCT is anticipated to be minimal. Surprisingly, however, vibrations attributable to both bipyridine and box moieties are evident. The feature at 1526 cm^{-1} associated with the phenolate ligand observed at 457.9 nm excitation is present, although at this excitation wavelength there can be no resonance with intraligand transitions. Furthermore, bands at 1435, 1358, 1265, and 1249 cm^{-1}, and features between 962 and 490 cm^{-1}, are enhanced at this wavelength. These modes are unaffected by deuteriation of the bipyridine ligands and are therefore attributed to box. The Ru−N feature apparent at 377 cm^{-1} with 457.9 nm excitation is now barely evident. This strongly suggests that the longest wavelength absorbance in this complex is associated with an interligand charge-transfer transition involving the phenolate and polypyridyl units. Such behavior has been described previously in hydroquinone bound Ru(bpy) units.[1,17,18] For $[Os(bpy)_2(box)]^+$, similar arguments may be made: 457.9 nm excitation leads to enhancement of the Os−N, bpy, and box modes. Excitation at 632.8 nm, however, leads to enhancement of broadly the same features; however, in this instance, the Os−N vibration remains. This is not surprising because 632.8 nm is also resonant with the low energy ^{3}Os(dπ)−bpy (π*) transition.

Figure 4b shows the Raman spectrum for $[Ru(biq)_2(box)]^+$ excited at 514 nm. Features at 1599, 1494, 1458, 1374, 1320, and and 772 cm^{-1} are typically associated with the biquinoline ligands,[19] and the band at 372 cm^{-1} is attributed to the Ru−N biquinoline vibration. This confirms that the electronic band centered at 600 nm is Ru (dπ)−biq (π*) MLCT. Bands at 1526 and 667 cm^{-1} observed in Figure 4 (inset), associated with box excitation, are not evident here. This is because this wavelength is too low in energy to be resonant with any intraligand box based transitions. In contrast, the Raman spectrum excited at 457.9 nm[20] reveals only box transitions, with no evidence for biq or metal based transitions. The 457.9 nm excitation is resonant with the box $\pi-\pi$* transition but not with MLCT transitions which occur at lower energy for the biquinoline based complex. This confirms that bands centered around 1609, 1525, 1461, 1433, 1367, 1347, and 1312 cm^{-1} are attributable to the ligand.

Excitation at 632.8 nm is resonant with both the long wavelength shoulder of $[Ru(biq)_2(box)]^+$ centered at 670 nm and the MLCT at 600 nm. This excitation results in enhancement of vibrational features at 1599, 1506, 1458, 1373, 1320, and 772 cm^{-1} associated with biquinoline but also strong enhancement of box features at 1526 and 670 cm^{-1} and weaker box features at 871, 807, and 629 cm^{-1}. The M−L vibrations observed at 514 nm excitation are of

(16) Strekas, T. C.; Gafney, H. D.; Tysoe, S. A.; Thummel, R. P.; Lefoulon, F. *Inorg. Chem.* **1989**, *28*, 2964.
(17) Hartl, F.; Snoeck, T. L.; Stufkens, D. J.; Lever, A. B. P. *Inorg. Chem.* **1995**, *34*, 3887.
(18) Keyes, T. E.; Forster R. J.; Jayaweera, P. M.; Vos, J. G.; McGarvey, J. J. *Inorg Chem.* **1998**, *22*, 5925.
(19) Akyuz, S.; Akyuz, T.; Davis, J. E. D. *Vib. Spectrosc*. **2000**, *22*, 11.
(20) See Supporting Information.

Table 2. Electrochemical Data

complex	solvent	$E_{1/2}$ M(II)/(III)	E_{ox} phenol	$E_{1/2}$ L-L	k_f (s^{-1})	k_b (s^{-1})	K_{eq}[a]
box (free ligand)	methanol[b]		0.58[c]				
$[Ru(bpy)_2(box)]^+$	acetonitrile	0.28	1.15[c]	−1.85, −2.11	2×10^6	1386	1500
$[Ru(bpy)_2(box)]^+$	methanol	0.23					
$[Os(bpy)_2(box)]^+$	acetonitrile	−0.13	1.00[c]	−1.80, −2.10	9×10^2	30.1	30
$[Os(bpy)_2(box)]^+$	methanol	−0.08					
$[Ru(biq)_2(box)]^+$	acetonitrile	0.49	1.36[c]	−1.3, −1.60	4×10^6	1925	1900
$[Ru(biq)_2(box)]^+$	methanol	0.44					

[a] K_{eq} of M(III)−O (phenoxy) bond after second oxidation process, obtained from k_f/k_b. [b] Electrochemistry carried out in methanol containing 0.1 M NaOH. [c] Irreversible.

lower relative intensity than those of the bipyridine based complexes. Therefore, longer wavelength excitation results in the appearance of box features indicating that the lowest energy transitions involve both the phenolate and biquinoline ligands.

An interesting conclusion derived from these spectroscopic studies is that the lowest energy electronic transition is an interligand charge transfer originating from the phenolate in the ruthenium complexes. The lowest energy transition in $[Os(bpy)_2(box)]^+$ appears to be the triplet MLCT transition which is superimposed on the ILCT.

The energies of the ILCT bands are strongly dependent on the nature of the counter ligands but are less influenced by the identity of the metal. Comparing $[Ru(bpy)_2(box)]^+$ to $[Ru(biq)_2(box)]^+$, the ILCT charge transfers are centered at approximately 550 and 670 nm, respectively. The lower energy of the latter transition is a result of the greater π-accepting ability of the biquinoline ligand compared with bpy and is consistent with the more anodic reduction potential of this site discussed vide infra.

The influence of the metal site on the ILCT is more difficult to assess as a result of difficulty in deconvoluting the electronic transitions from the $[Os(bpy)_2(box)]^+$ spectrum. However, it would appear that the ILCT in the Os based complex is similarly placed compared to that of its Ru analogue.

Electrochemistry. Spectroscopic studies indicate that the lowest energy singlet electronic transitions in the reduced complexes are phenolate (π)−bpy (π^*). This suggests that the site of most facile oxidation in these complexes should be the phenolate ligand. Such spectroscopy has been observed in Ru(II) catecholate and hydroquinone based systems, and indeed, the ligands are the sites of the most facile oxidation.[1,32]

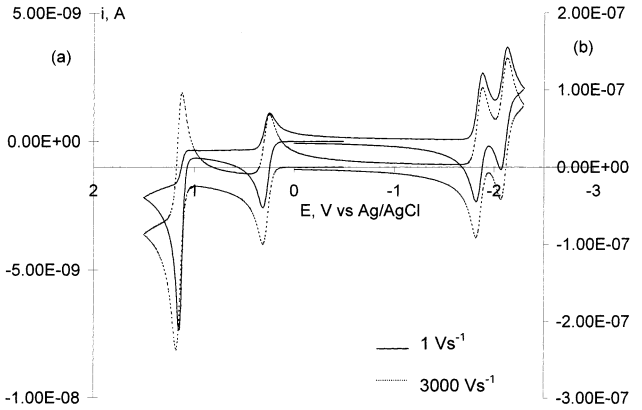

Figure 5. Scan rate dependent cyclic voltammetry of $[Ru(bpy)_2(box)]^+$ conducted in acetonitrile containing 0.1 M tetraethylammonium tetrafluoroborate on a 5 μm electrode, potentials are versus Ag/AgCl electrode.

The electrochemical data from the discussed complexes are shown in Table 2. Figure 5 illustrates the voltammetry of $[Ru(bpy)_2(box)]^+$, in acetonitrile at scan rates of 1 and 3000 V s^{-1}. Two oxidations are observed for this complex, a reversible one-electron oxidation at 0.28 V and an irreversible one-electron process at 1.15 V. Two reversible one-electron reductions are observed at −1.85 and −2.11 V versus Ag/AgCl and are assigned, from consideration of comparable materials, to the reduction of the bipyridine moieties. The spectroelectrochemistry of the complexes discussed is described in detail in the following section, and suggests, surprisingly, on the basis of the spectroscopy of the reduced complex, that the first oxidation is metal based. We attribute the second wave to the oxidation of the phenol site, on the basis of the spectroelectrochemistry described vide infra and the oxidation potential of the free deprotonated box ligand which exhibits an irreversible oxidation in methanol at 0.58 V at a scan rate of 0.1 V s^{-1}.

The behavior of the phenolate oxidation wave in $[Ru(bpy)_2(box)]^+$ is dependent on scan rate, being irreversible at slower scan rates, and becoming reversible only at scan rates in excess of 500 V s^{-1}. Repetitive scans and scan rate dependence show no indication of adsorption or other surface phenomena common in phenols, which may be associated with this irreversible behavior. At 1.15 V, the metal is already

(21) As the decomposition reaction is first order, $t_{1/2} = \ln 2/k_f$.
(22) Goldsby, K. A.; Meyer, T. J. *Inorg. Chem.* **1984**, *23*, 3002.
(23) Hage, R.; Haasnoot, J. G.; Nieuwenhuis, H. A.; Reedijk, J.; DeRidder, D. J. K.; Vos, J. G. *J. Am. Chem. Soc.* **1990**, *112*, 9245.
(24) Nazeeruddin, M. K.; Zakeeruddin, S. M.; Kalyanasundaram, K. *J. Phys. Chem.* **1993**, *97*, 9607.
(25) Tang, J.; Albrecht, A. C. *Raman Spectroscopy*; Szynanski, H., Ed.; Plenum Press: New York, 1970; Vol. 2.
(26) See Supporting Information.
(27) Manuscript in preparation.
(28) (a) Vogler, A.; Kunkely, H. *Comments Inorg. Chem.* **1990**, *9*, 201 (b) Vogler, A.; Kunkely, H. *Comments Inorg. Chem* **1997**, *19*, 283.
(29) (a) Cummings, S. D.; Eisenberg, R. J. *Am. Chem. Soc.* **1996**, *118*, 1949. (b) Connick, W. B.; Gray, H. B. *J. Am. Chem. Soc.* **1997**, *119*, 11620. (c) Paw, W.; Lachicotte, R. J.; Eisenberg, R. *Inorg. Chem.* **1998**, *37*, 4141
(30) Da Silva, R. S.; Gorelsky, S. I.; Dodsworth, E. S.; Tfouni, E.; Lever, A. B. P. *J. Chem. Soc., Dalton Trans.* **2000**, 4078.
(31) Masui, H.; Lever, A. B. P., Dodsworth, E. S. *Inorg. Chem.* **1993**, *32*, 258.
(32) Lever, A. B. P.; Masui, H.; Metcalfe, R. A.; Stufkens, D. J.; Dodsworth, E. S.; Auburn, P. R. *Coord. Chem. Rev.* **1993**, *125*, *317*.

in the 3+ state, and irreversibility in the following oxidation wave is attributed to the decomposition of the electron poor Ru(III)−O (phenoxy) bond. Such behavior has been reported for Ru(III)−O (quinone) bonds.[18,1] At faster scan rates, the phenol oxidation becomes reversible, suggesting relatively slow decomposition of the complex, which is outrun at scan rates in excess of 500 V s^{-1}.

The equilibrium constant for formation of the decomposed material provides a useful means of quantifying and comparing the relative influences of counter ligand and metal on the stability of the M(III)−O (phenoxy) bond. We have, therefore, fitted the scan rate dependent cyclic voltammograms to a mechanism in which electron transfer, E, is followed by a chemical reaction, C. In fitting this EC mechanism, we assume that the product of the following reaction is not electroactive at potentials where the parent complex is being oxidized. This fitting approach yields rate constants for the forward and backward steps that are consistent across a wide range of scan rates. Table 2 contains these rate constants for the following chemical reactions and estimates of K_{eq} obtained from these data whereby $K_{eq} = k_f/k_b$, where k_f is the forward and k_b is the reverse rate constant. Fitting the CV of $[Ru(bpy)_2(box)]^+$ to an EC mechanism yields a decomposition half-life of approximately 5×10^{-4} s^{-1} and an estimate of K_{eq} of 1500.[21]

The electrochemical data for $[Os(bpy)_2(box)]^+$ are presented in Table 2. $[Os(bpy)_2(box)]^+$ exhibits an initial oxidation at −0.13 V versus Ag/AgCl which is in excess of 400 mV cathodic of its Ru analogue. This would appear to confirm the metal based nature of these first oxidations. Such shifts are typically observed across many groups of analogous Ru and Os complexes and are associated with the higher energy of the 5d orbitals in Os compared with the 4d orbitals in Ru.[22] Bipyridyl reductions are observed at −1.8 and −2.10 V. For the Os complex, the phenolate oxidation appears at a potential 150 mV cathodic of the Ru analogue. This also appears to confirm the assignment of the second oxidation wave for these two complexes because the 150 mV difference is less than expected between Ru and Os metal oxidations, but it reflects the impact of metal identity on the phenol site.

The phenol oxidation exhibits greater chemical reversibility for the osmium complex than its Ru analogue, exhibiting full reversibility at a scan rate of 20 V s^{-1}. K_{eq} is estimated to be 30, and this material has shows a relatively slow decomposition of the Os(III)−O$^\bullet$ bond with a half-life for decomposition of approximately 0.023 s^{-1}. This implies greater M(III)−O stability in the Os complex.

There are relatively few reports of phenolate bound Ru and Os(II) complexes in the literature. Where complexes with comparable electrochemistry have been reported, the second oxidation wave has been attributed to the M(IV)/(III) couple.[2,3] In the complexes discussed here, we conclude that the second oxidation is attributed to the phenol. First, because in basic media the deprotonated box ligand is oxidized irreversibly at 0.58 V, and in neutral media the potential of this irreversible wave is approximately 1.1 V. Conversely, the M(III)/M(IV) couple is rarely observed in normal potential windows, even for complexes bearing strong donor ligands[23] and is therefore unlikely to precede the phenolate oxidation in these complexes. Second, as described, the potential difference in the metal based oxidation waves of $[Ru(bpy)_2(box)]^{2+}$ and $[Os(bpy)_2(box)]^{2+}$ is 410 mV compared with a 150 mV difference between the second oxidation processes. The former potential difference is typical of that observed for other Ru/Os analogues, and if the second wave were due to a metal process, a comparable potential difference between Ru and Os would be anticipated.

$[Ru(biq)_2(box)]^+$ exhibits the most anodic oxidations of the three complexes studied. The first, reversible, oxidation wave is apparent at 0.49 V. The first reduction step for this complex, sited at the biquinoline, is observed at −1.30 V. The strong π-accepting ability of this ligand is reflected in the ease with which it is reduced and is responsible for the reduced electron density at the metal and phenolate sites resulting in the anodic shift in the associated oxidations. The second oxidation at 1.36 V is anodically shifted and considerably less reversible by comparison with $[Ru(bpy)_2(box)]^+$ and $[Os(bpy)_2(box)]^+$, requiring scan rates in excess of 3000 V s^{-1} for a reversible response. K_{eq} for decomposition of $[Ru(biq)_2(box)]^{2+}$ was determined to be 1900 ($t_{1/2} = 3.6 \times 10^{-4}$ s^{-1}), the largest equilibrium constant for the three complexes reflecting the lability of its oxidized state. The assignments of the first and second redox steps in this complex, on first examination, appear to be metal and phenol based, respectively, as for the $[M(bpy)_2(box)]^+$ based complexes. Spectroelectrochemical data, provided vide infra, indicate strong mixing, and the formal assignment of the sequence of oxidation steps is less clear. However, whether it is the metal or ligand which is oxidized first, the final oxidized product should remain the same, and the irreversibility of the second oxidative process is still attributed to decomposition of the electron poor Ru(III)−O$^\bullet$ bond.

The reversibility of the phenolate oxidation wave is a useful guide to the electron density on metals and ligands in these systems. $[Os(bpy)_2(box)]^+$ exhibits the most cathodic oxidations on both metal and ligand sites. The phenolate oxidation shows the greatest reversibility in this complex and the slowest rate of decomposition when the system is oxidized. The greater electron density available to the Os site and its increased propensity for π-back-donation is likely to contribute to the relative ease of oxidation of the phenolate and the enhanced stability of the Os(III)−phenoxy radical species. This contrasts with the $[Ru(biq)_2(box)]^+$ complex which exhibits a large anodic shift in both oxidation processes and significantly less reversibility in the oxidation step. In this instance, the strong π-accepting ability of the biquinoline moieties forces oxidations to higher potentials and strips electron density from the Ru(III)−O, reducing the stability of this bond.

Spectroelectrochemistry. To investigate the electrochemical processes further, potential controlled electronic and resonance Raman spectroscopy was conducted. The Raman spectroelectrochemistry of the complexes is shown in dichloromethane, because this solvent interfered least with the M−L transitions which appear between 350 and 400 cm^{-1} and are useful in assessing the involvement of the metal in

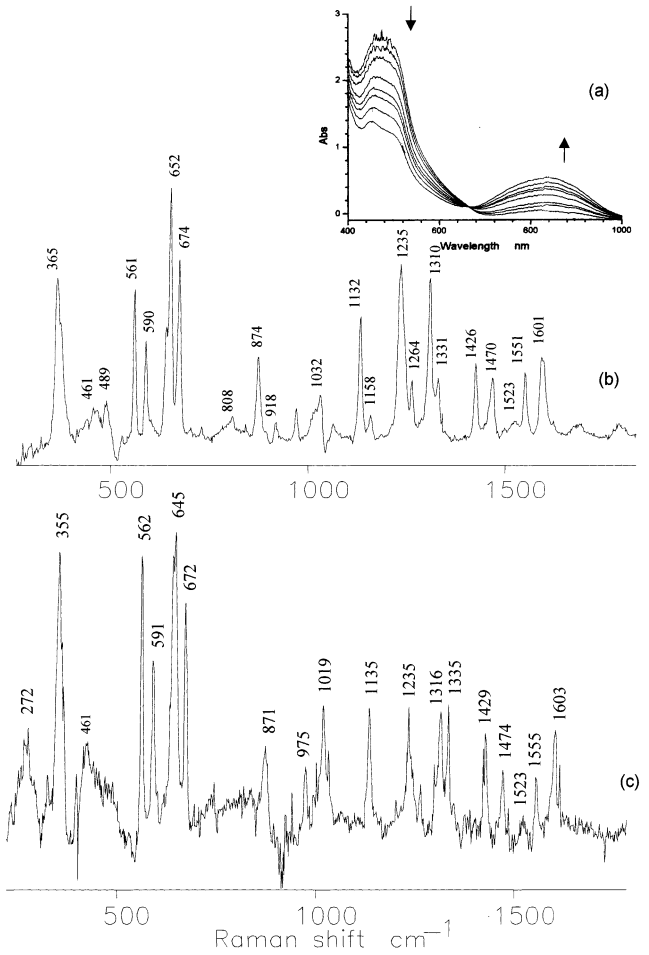

Figure 6. Controlled potential spectroscopy of (a) $[Ru(bpy)_2(box)]^+$ electronic spectroscopy, (b) $[Ru(bpy)_2(box)]^+$ resonance Raman spectroscopy in dichloromethane, excited at 785 nm, and (c) resonance Raman of $[Os(d_8\text{-bpy})_2(box)]^+$ in dichloromethane, excited at 785 nm. The applied potential in each instance was 0.5 V vs Ag/AgCl, and the electrolyte was 0.1 M tetraethylammonium tetrafluoroborate.

optical transitions. Changing the solvent in this way does not alter the spectra significantly.

The electronic spectroelectrochemistry of $[Ru(bpy)_2(box)]^+$ is shown in Figure 6a. Holding the applied potential at 0.4 V, the main feature at 488 nm is lost with concomitant growth of an intense new band centered at 850 nm. A new feature also grows in at 310 nm which is typical of Ru(III) formation The 850 nm band is thought to be an LMCT transition. Because the most facile oxidation for this complex lies on the phenolate group in this instance and not on a bipyridine, it seems likely that the transition observed is phenolate (n) to Ru(III) ($d\pi^*$). In polypyridyl systems such as $[Ru(bpy)_3]^{3+}$, the LMCT, bpy (π) to Ru ($d\pi^*$), is a very weak transition centered at approximately 675 nm.[24] The intensities of such transitions are strongly influenced by the reducing ability of the donor ligand. The LMCT transition reported here is intense and red-shifted by comparison with bipyridine based transitions.

The optical changes associated with the first oxidation step for all complexes described are entirely reversible. Consistent with the electrochemical studies described previously, bulk electrolysis of the complexes at their second oxidation potentials results in irreversible decomposition.

Resonance Raman spectroscopy of the oxidized complexes was carried out to confirm the identity of the new optical transition at 850 nm. Figure 6b shows the Raman spectrum of $[Ru(bpy)_2(box)]^{2+}$ excited at 785 nm which is resonant with this absorption.

The spectroscopy is rich; enhanced features appear at 1601, 1551, 1523, 1470, 1426, 1331, 1310, 1264, 1235, 1158, 1132, 970, 918, 874, and 808 cm^{-1} which are attributed to the box ligand C−C and ring stretch modes. Vibrations at 674, 652, 590, and 561 cm^{-1} are strongly enhanced and are attributed to Ru−O bridge coupled modes; similar vibrations have been described in other oxygen coordinated Ru complexes.[1,18] The relative intensity of these features suggests that the optical transition results in significant distortion around the Ru−O bond.[25] Bands at 365 and 461 cm^{-1} are attributed to Ru(III)−N(box) and Ru−O(box), respectively; the shift of the Ru−N from 372 cm^{-1} in $[Ru(bpy)_2(box)]^+$ to 365 cm^{-1} for $[Ru(bpy)_2(box)]^{2+}$ is indicative of the oxidation of the metal. Clearly, the appearances of metal−ligand and metal−ligand bridge coupled modes indicate the metal is participating in the electronic transition. There is, however, no evidence for the participation of the bipyridyl moieties in this transition. Therefore, the 850 nm band is attributed to a phenolate (π) to Ru(III) ($d\pi$), LMCT, transition. Finally, the Raman spectrum of $[Ru(bpy)_2(box)]^{2+}$ was also investigated exciting at 457.9 nm, where formerly the MLCT transition had been identified in the reduced species.[26] Oxidation results in complete loss of the bpy bands associated with the MLCT transition. However, bands associated with the box ligand do remain, because of some degree of resonance with the $\pi-\pi$ transition of the ligand. This observation again confirms the metal-based nature of the first oxidation of $[Ru(bpy)_2(box)]^+$. The electronic spectroelectrochemistry of $[Os(bpy)_2(box)]^+$ is similar to that of $[Ru(bpy)_2(box)]^+$. Holding the potential at 0.4 V results in loss of the MLCT transition and formation of a new electronic transition at 830 nm. Figure 6c shows the resonance Raman spectrum of $[Os(d_8\text{-bpy})_2(box)]^{2+}$ excited at 785 nm. The similarities between this spectrum and that in Figure 6b are remarkable. Vibrations of common origin for both complexes are observed at 562, 591, 672, 871, 975, 1019, 1132, 1158, 1235, 1263, 1316, 1330, 1429, 1474, 1555, and 1603 cm^{-1}. The small differences that are observed correspond to the different metal identities; for example, the M(III)−N vibration occurs at 355 cm^{-1} for Os compared with 365 cm^{-1} for Ru, and M−O bridge coupled modes occur at 645 cm^{-1} for Os and 652 cm^{-1} for Ru. The similarities in Figure 6b,6c confirm two points: First, the electrochemical behavior of $[Ru(bpy)_2(box)]^{2+}$ and $[Os(bpy)_2(box)]^{2+}$ is analogous; that is, the metal is the site of primary oxidation. Second, the Raman spectrum shown in Figure 6c corresponds to the complex in which the bipyridyl units are perdeuteriated. Despite this, the spectra in Figure 6b,c are essentially identical. If bipyridyl were involved in the NIR transition for the oxidized complex, shifts of up to 60 cm^{-1} in the bpy based vibrations would be expected on deuteriation.[18] That no shifts are observed

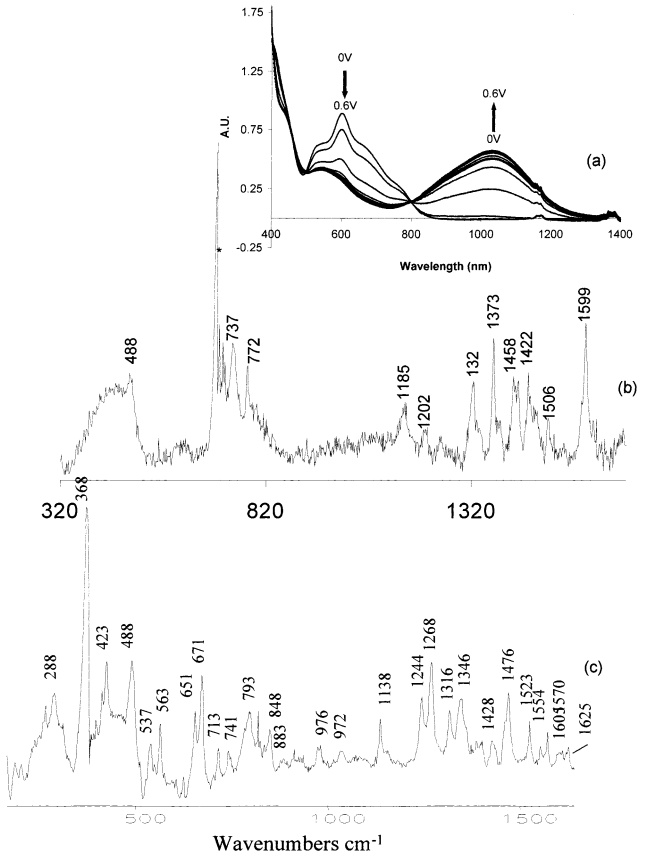

Figure 7. Controlled potential spectroscopy of (a) $[Ru(biq)_2(box)]^+$ electronic spectroscopy, (b) resonance Raman of $[Ru(biq)_2(box)]^+$ in dichloromethane, excited at 514 nm, and (c) resonance Raman of $[Ru(biq)_2(box)]^+$ in dichloromethane, excited at 810 nm. The applied potential in each instance was 0.6 V vs Ag/AgCl, and the electrolyte was 0.1 M $TeaBF_4$.

unambiguously confirms that the bipyridyl unit does not participate in the this optical transition. Because the metal is oxidized, and the phenolate is a good donor, we assign the NIR band for $M(bpy)_2$ containing complexes as a phenolate (π) to M(III) (dπ), LMCT transition.

The assignments of optical transitions in $[Ru(biq)_2(box)]^+$ are somewhat less clear. The spectroelectrochemistry and corresponding resonance Raman spectroscopy for $[Ru(biq)_2(box)]^+$ are shown in Figure 7. Figure 7a reveals that the first oxidation step of this complex results in loss of the long wavelength shoulder at 670 nm and a significant decrease in the intensity of the transitions centered at 600 nm. Concomitantly, an intense, broad new transition appears at 1100 nm. An isosbestic point is maintained throughout the oxidation at 790 nm.

Resonance Raman spectroscopy, exciting the oxidized complex at 514 nm, reveals little change by comparison with Figure 4b, although the relative intensity of the Ru−N vibration at 377 cm^{-1} is significantly reduced. Raman spectra were recorded using 810 nm excitation, which is resonant with NIR absorbance of the oxidized complex at 1100 nm. Comparison of this spectrum with the resonance Raman spectra of $[Ru(bpy)_2(box)]^{2+}$ and $[Os(bpy)_2(box)]^{2+}$ excited at 785 nm reveals some differences. This is surprising because if the metal is oxidized first in $[Ru(biq)_2(box)]^{2+}$ the resulting optical transitions should originate from the same chromophores for each complex. Hence,the Raman spectra, generated by excitation into these bands, would be expected to be identical across all three compounds. Furthermore, if the NIR transitions for $[Ru(bpy)_2(box)]^{2+}$ and $[Ru(biq)_2(box)]^{2+}$ are the same, the 250 nm difference between the band maxima seems rather large but may be associated with the electron withdrawing nature of the biquinoline ligand.

Enhanced vibrations are observed at 423, 537, 713, 741, 793, 848, 1268, 1346, 1570, and 1625 cm^{-1}, for which there are no comparable bands in the Raman spectra of $[M(bpy)_2(box)]^{2+}$. Furthermore, these bands are not ascribed to biquinoline. Bands centered at 488, 563, 651, and 671 cm^{-1} are common to all three spectra and are attributed to box and Ru−O box coupled vibrations. Similarly, bands at 916, 972, 1138, 1244, 1268, 1316, 1476, 1554, and 1605 cm^{-1} are tentatively attributed to C−C vibrations in the phenyl ring of the box ligand. Given the strong similarities in the resonance Raman spectra of the LMCT for $[M(bpy)_2(box)]^{2+}$, the differences between these spectra and that of $[Ru(biq)_2(box)]^{2+}$ is unexpected and indicates that the optical transition at 1100 nm may not be simply an LMCT transition. The electrochemistry and Raman spectroscopy of this complex excited at 514 nm are suggestive of metal oxidation, whereas the vis−NIR spectroelectrochemistry and Raman spectroscopy of $[Ru(biq)_2(box)]^{2+}$ excited at 810 nm suggest that the phenol may be oxidized. These contradictory observations may be attributed to strong mixing between phenol and ruthenium orbitals. However, the large bandwidth of the 1100 nm transition excludes the possibility that the metal−phenolate orbitals are entirely delocalized.

Photochemical Stability. An issue that may be important if these complexes are to be of utility in photovoltaic devices is their photostability.

Photolysis studies were conducted on all three complexes under continuous visible irradiation in the following media: dichloromethane, dichloromethane containing 0.1 M LiCl, acetonitrile, and acetonitrile containing 0.1 M LiCl. In all instances, changes of less than 10% in the absorption spectra of the complexes were observed over a 4 h period. This photostability is most likely attributable to the fact that the complexes have short-lived excited states[27] compared with the rate of decomposition of the complex, which electrochemical studies (vide supra) would indicate to be slow. Furthermore, the strong σ-donor properties of the phenolate may contribute to a large crystal field splitting, resulting in a thermally inaccessible ^{3}MC state, thus avoiding photodecomposition. Such photostability has been observed in other Ru complexes, containing strong σ-donors such as triazolates.[7]

Comparison of Redox and Spectroscopic Orbitals. Interligand charge-transfer transitions are relatively uncommon, and it is only in recent years that they have been studied to any significant degree.[28] Observation of ILCT bands depends on the simultaneous presence of strong donor and acceptor ligands within the one complex. Coupling of these sites, possibly through mediation of the metal, may result in a charge-transfer transition. Work has focused most notably

Scheme 2. Schematic Illustrating Relative Energies of Metal and Ligand Orbitals of $[Ru(L\text{-}L)_2(box)]^+$ as Indicated by Electrochemical and Spectroscopic Data

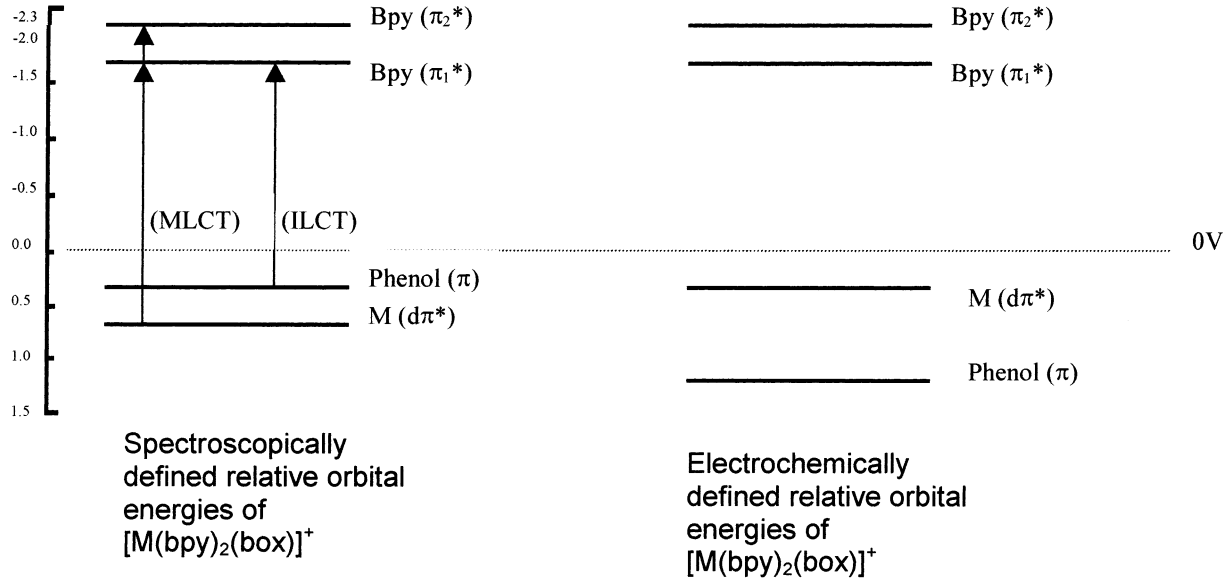

to date on complexes containing diimine and dithiolate ligands,[29] although some reports have also been made on diimine and hydroquinone complexes. In Ru and Os O^- bound hydroquinone complexes, these transitions have been observed at lower energy than the MLCT transition.[18,30−33] In such complexes, the donating hydroquinone or catechol ligand is oxidized at potentials that are cathodic of the associated metal. This is not surprising because the electronic absorption energies and ground state redox potentials have been shown to correlate linearly across a broad range of Ru and Os polypyridyl complexes.[34−37] This strong correlation has been attributed to the participation of the same ligand π^* orbital in the first reduction and lowest energy optical transition. This correlation has been subsequently cited and accepted as a useful means of predicting emission maxima and calculating excited state redox potentials and nonradiative decay constants for Ru and Os diimine complexes on the basis of ground state electrochemical properties, and it has been broadly successful in estimating such parameters.[38]

To our knowledge, this is the first report identifying diimine phenolate ILCT transitions.

A particularly interesting feature of the complexes discussed is that the lowest energy optical transition originates from the phenolate whereas the first oxidation originates on the metal. Considerable literature is available on comparative studies of redox and spectroscopic orbitals for Ru(II) and Os(II) complexes.[39−41] In the vast majority of cases, strong correlations exist, and redox and optical processes are presumed to originate from the same orbitals. That is, in general, the most easily oxidized ligand is identified as the site of the LUMO, and the metal site of most facile oxidation is the HOMO. The complexes described here appear to provide exceptions to this general observation.

In each instance for $[M(bpy)_2(box)]^{2+}$, the primary oxidation originates at the metal site. The ligand oxidation occurs some 800−1000 mV positive of the metal oxidation. However, it is important to remember that this oxidation is artificially anodic as it corresponds to a phenolate bound to an M(III) and not an M(II) center.

Electronic and resonance Raman spectroscopy suggests that the lowest energy optical transition is attributable to a phenolate (π) to bpy (π^*) ILCT for each complex. Comparable electronic spectroscopy has been discussed previously for Ru and Os complexes, bound through the oxygen moiety to hydroquinone.[17,18] However, in these instances, the primary oxidation occurred correspondingly, on the ligand.

Therefore, a clear disparity exists between what are electrochemically and spectroscopically assigned as the HOMO for these phenolate complexes. The origins of this discrepancy are unclear, and to our knowledge, this is one of the very few examples of this behavior reported. Scheme 2 provides a simple illustration of the relative orderings of the orbitals as indicated by electrochemical and spectroscopic data for $[Ru(bpy)_2(box)]^{2+}$. The diagrams are constructed under the assumption that the bipyridine reduction potentials are unchanged between electrochemical and spectroscopic orbitals. On the basis of the electrochemical data, one would expect that the MLCT would be the lowest energy transition for these complexes. However, from spectroscopic data and the bpy reduction potential, we estimate the phenolate oxidation potential, when bound to Ru(II), to be approximately 0.2 V.[42] As described, the potentials of the

(33) Ebadi, M.; Lever, A. B. P. *Inorg. Chem.* **1999**, *38*, 467.
(34) Ernst, S.; Kaim, W. *Inorg. Chem.* **1989**, *28*, 1520.
(35) DeArmond, M. K.; Carlin, C. M. *Coord. Chem. Rev.* **1981**, *36*, 325.
(36) Vlcek, A. A. *Coord. Chem. Rev.* **1982**, *43*, 39.
(37) Dodsworth, E. S.; Lever, A. B. P. *Inorg. Chem.* **1990**, *29*, 499.
(38) Dodsworth, E. S.; Lever, A. B. P. *Chem. Phys. Lett.* **1986**, *124*, 152.
(39) Juris, A.; Barigelletti, F.; Campagna, S.; Balzani, F.; Belser, P.; von Zelewsky, A. *Coord. Chem. Rev.* **1988**, *84*, 85.
(40) Ohsawa, Y.; Hanck, K. W.; De Armond, M. K. *J. Electroanal. Chem. Interfacial Electrochem.* **1984**, *175*, 229.
(41) (a) Heath, G. A.; Yellowlees, L. J.; Braterman, P. S. *J. Chem. Soc., Chem. Commun.* **1981**, 287. (b) Heath, G. A.; Yellowlees, L. J.; Braterman, P. S. *Chem. Phys. Lett.* **1982**, *92*, 66.

(42) Calculated from the bipyridyl reduction, −1.85 V.

second, phenolate, oxidation step are artificially high as a consequence of the preceding step. This suggests that the metal and phenolate orbitals are closely matched energetically. Semiempirical calculations on $[Ru(bpy)_2(box)]^+$, described later, also lend support to this conclusion, whereby the HOMO appears to have both metal and ligand contributions. What determines which state the electron will originate from under electrochemical and optical conditions is currently unclear but may be related to strong metal mediated coupling of phenolate and bpy π^*_1 orbitals which facilitates the optical transitions.

The nature of the first oxidation in the $[Ru(biq)_2(box)]^+$ complex is somewhat ill-defined. Its electrochemical behavior is reminiscent of a metal-based process; however, spectroelectrochemistry (both UV−vis and resonance Raman) suggest that the MLCT transition may be retained after oxidation. The resonance Raman spectrum of the new optical transition at 1100 nm is quite different from the phenolate to Ru LMCT observed for $[Ru(bpy)_2(box)]^{2+}$ and $[Os(bpy)_2(box)]^{2+}$. The uncertain identity of the first oxidation in $[Ru(biq)_2(box)]^+$ is attributed to strong mixing of metal/phenolate orbitals in this complex. The oxidation potential of the metal in this complex is anodic by comparison with the bpy based complexes as a result of the greater π-accepting ability of the biquinoline. This is likely to narrow the energy gap between the phenolate and metal based orbitals even further, as the oxidation potential of $[Ru(biq)_2(box)]^+$ is 0.49 versus 0.58 V for the free phenolate. The phenol and metal based orbitals are therefore likely to be very closely matched energetically and hence strongly mixed, rendering formal assignment of oxidation and spectroscopic processes difficult. This level of strong mixing between metal and ligands has been observed in other ligands containing O donors such as quinones and catecholates, where mixing was similarly attributed to comparable metal−ligand orbital energies.[32,33] However, in such complexes, the ligand is itself most easily oxidized and results in the generation of new MLCT transitions.

A useful means of identifying the extent of localization in the chromophores in such transitions is to study the solvent dependence. The 1100 nm absorbance for $[Ru(biq)_2(box)]^+$ is only moderately solvent dependent showing a blue shift of approximately 10 nm between acetonitrile and dichloromethane. Previous reports of strongly mixing systems have also identified relatively small solvent shifts. In such cases, there is apparently a limited change in the dipole moment between the ground and excited states.

Semiempirical Calculations. In an attempt to gain further insight into the extent of metal−ligand orbital mixing in these systems, the electronic spectrum of the complex was calculated by semiempirical ZNDO (INDO/S-CI) techniques, using the crystal data for the energy minimized structure. The theoretical results corresponded reasonably well with the experimental results. For $[Ru(bpy)_2(box)]^+$, a band at 465 nm and transitions with lower oscillator strengths above 500 nm were calculated. The electronic structure of $[Ru(bpy)_2(box)]^+$ in the ground state features a large contribution from both the Ru atomic orbitals and the box ligand orbitals to the HOMO. The box ligand orbital is polarized toward the phenolate part. On the other hand, the LUMO is largely dominated by the contributions coming from the bpy ligands, which is consistent with the electrochemical results described previously. The calculated electron density plots are shown in the Supporting Information. Calculations based on the ruthenium (III) complex were only partly successful, because the spectroelectrochemical data were rather poorly reproduced partly because of the geometry changes accompanying oxidation and also because of the absence of suitable parameters for the Ru^{3+} ion.

Conclusions

The synthesis and characterization of a series of Ru and Os diimine complexes O,N bound to a 2-(2-hydroxyphenyl)-benzoxazole are reported. Electronic spectroscopic and resonance Raman studies indicate that the lowest singlet optical transition is a phenolate to diimine interligand charge-transfer transition in all cases. Electrochemistry indicates, however, that the first oxidation involves a M(II)/M(III) couple for $[M(bpy)_2(box)]^+$. This behavior contrasts with a large range of studies on Ru and Os, which have shown that the HOMO and LUMO assignments may be made from electrochemical data; we discuss this apparent disparity in terms of metal−ligand and ligand−ligand orbital mixing. Oxidation of these complexes results in an intense NIR transition ascribed to a LMCT phenolate (π)−M(III) (dπ). The behavior for $[Ru(biq)_2(box)]^+$ is less well defined. The lowest energy optical transition is assigned as ILCT in character. However, the first oxidation step in this case would appear to involve both metal and ligand, suggesting extensive metal−phenolate orbital mixing in this complex. Oxidation of the biquinoline complex results in an intense transition centered at 1100 nm which appears to be different in nature from those observed for $[M(bpy)_2(box)]^{2+}$. Strong metal−phenol orbital mixing is implicated, and this seems to be corroborated by the closer energy match between the phenolate and metal redox levels. We employ dynamic electrochemistry to assess the stability of the second oxidation step in these complexes and find that it provides a useful correlation with the electron donor and acceptor abilities of both metal and ligands in the complex.

In all, this work illustrates some interesting anomalies in relatively simple complexes, which are attributed to the proximity of ligand and metal orbital energy levels. Such ambiguity in electronic charge distribution is reminiscent of the behavior of ruthenium quinoid complexes and suggests that phenol based complexes may also show some of the same complexity of behavior. This work illustrates how simple synthetic alterations may be employed to tune the spectroscopic range over which a number of intense visible and NIR absorbances occur. These complexes have also enabled examination of the behavior of the metal site when bound to an O^- donor, which remains reduced over the full range of oxidation potentials of the metal.

Acknowledgment. T.E.K. and D.L. acknowledge the DIT Scholarship scheme for funding. T.E.K. and R.J.F. acknowl-

edge the generous loan of Ru and Os salts from Johnson Matthey. T.E.K. and D.L. acknowledge FOCAS, DIT, and the Higher Education Authority under which FOCAS is funded under the National Development Plan 2000 to 2006. C.G.C. and J.J.McG. acknowledge the EPSRC for funding under Grant GR-M45696.

Supporting Information Available: Resonance Raman spectra of $[Ru(biq)_2(box)]^+$ excited at 457.9 nm. Semiempirical ZNDO (INDO/S-CI) calculated electron density plots for the HOMO and LUMOs of $[Ru(bpy)_2(box)]^+$. This material is available free of charge via the Internet at http://pubs.acs.org.

IC0202561